A Coupled Ocean–Atmosphere System of SST Modulation for the Indian Ocean*

JOHANNES LOSCHNIGG[+] AND PETER J. WEBSTER

Program in Atmospheric and Oceanic Sciences, University of Colorado, Boulder, Colorado

ABSTRACT

The net heat flux into the northern Indian Ocean is between 75 and 100 W m^{-2} during the boreal spring and early summer but only 10–20 W m^{-2} in the western Pacific during the entire year. The differences in the net surface heat fluxes arise from the radiation shielding by deep convective clouds over the western Pacific and the near absence of clouds over the northern Indian Ocean during spring. Despite the strong heat flux during the boreal spring and early summer, the northern Indian Ocean only warms by 3°C over a 4-month period, much smaller than the 12°C estimated using single ocean column models. Similarly, the cooling of the North Indian Ocean during the boreal winter is less than can be explained from thermodynamic processes. The tropical western Pacific Ocean sea surface temperature (SST), on the other hand, varies by only 1°C throughout the year.

Despite the different net surface fluxes of heat into the two warm pools, the magnitude of the annual cycle of SST in each basin is very small and is confined to lie between 26° and 30°C. It is argued that SST regulation in the Pacific Ocean occurs as a combination of local thermodynamic balance with significant contributions from large-scale atmospheric circulations forced by SST gradients. On the other hand, the northern Indian Ocean SST is regulated by strong oceanic advection across the equator, southward during the boreal spring and early summer and northward during the boreal winter, and by changes in heat storage of the upper ocean. Cross-equatorial transports of heat vary from 0.5 PW southward in spring to 1.5 PW in summer. During the boreal winter, the heat fluxes reverse, averaging about 1 PW toward the north. Large oscillations of ocean heat transport are also noted on timescales of 20–50 days. It is concluded that ocean heat transports are an essential process in the annual cycle of the Indian Ocean heat balance. Last, the results of the study are used to propose a coupled ocean–atmosphere dynamic regulatory system for the annual cycle of the monsoon and the SST in the Indian Ocean.

1. Introduction

One of the intriguing features of the present climate is that the sea surface temperature (SST) of the tropical oceans peak near 30°C (302–303 K). These maxima occur in the so-called warm pools of the western Pacific Ocean and eastern and northern Indian Ocean (Fig. 1a). The Pacific Ocean warm pool is collocated with outgoing longwave radiation (OLR) minima (Fig. 1b), indicating deep convection and strong atmospheric heating. Such heating (together with polar cooling) drives the global climate and is an essential part of the El Niño–Southern Oscillation (ENSO) phenomena and the Asian–Australian monsoon (Webster 1994; Webster et al. 1998). Furthermore, small changes in the Pacific warm pool SST have been shown to create major perturbations in the tropical circulation and the climate far removed from the Tropics (e.g., Palmer and Mansfield 1984, among others). The sensitivity of climate to the warm pool SST is related to the nonlinear increase of surface saturated vapor pressure with SST, such that small changes in the SST near its maximum values invoke larger changes in evaporation and the subsequent release of latent heat than that produced by similar perturbations where the SST is cooler (Webster 1994). Given the importance of the warm pool to global climate and the sensitivity of climate to small changes in warm pool temperature, it is not surprising that there have been many efforts to understand the processes that regulate the maximum SST in the tropical warm pools. These questions have become particularly important as the tropical Pacific Ocean has been the focus of efforts to predict climate variability on the timescale of months to years (National Research Council 1994).

The international Tropical Ocean and Global Atmosphere Program (TOGA) was organized to understand the influence of the tropical oceans on climate and climate

---

[+] Current affiliation: International Pacific Research Center, University of Hawaii at Manoa, Honolulu, Hawaii.

Corresponding author address: Dr. Johannes Loschnigg, IPRC/SOEST, University of Hawaii at Manoa, Honolulu, HI 96822.
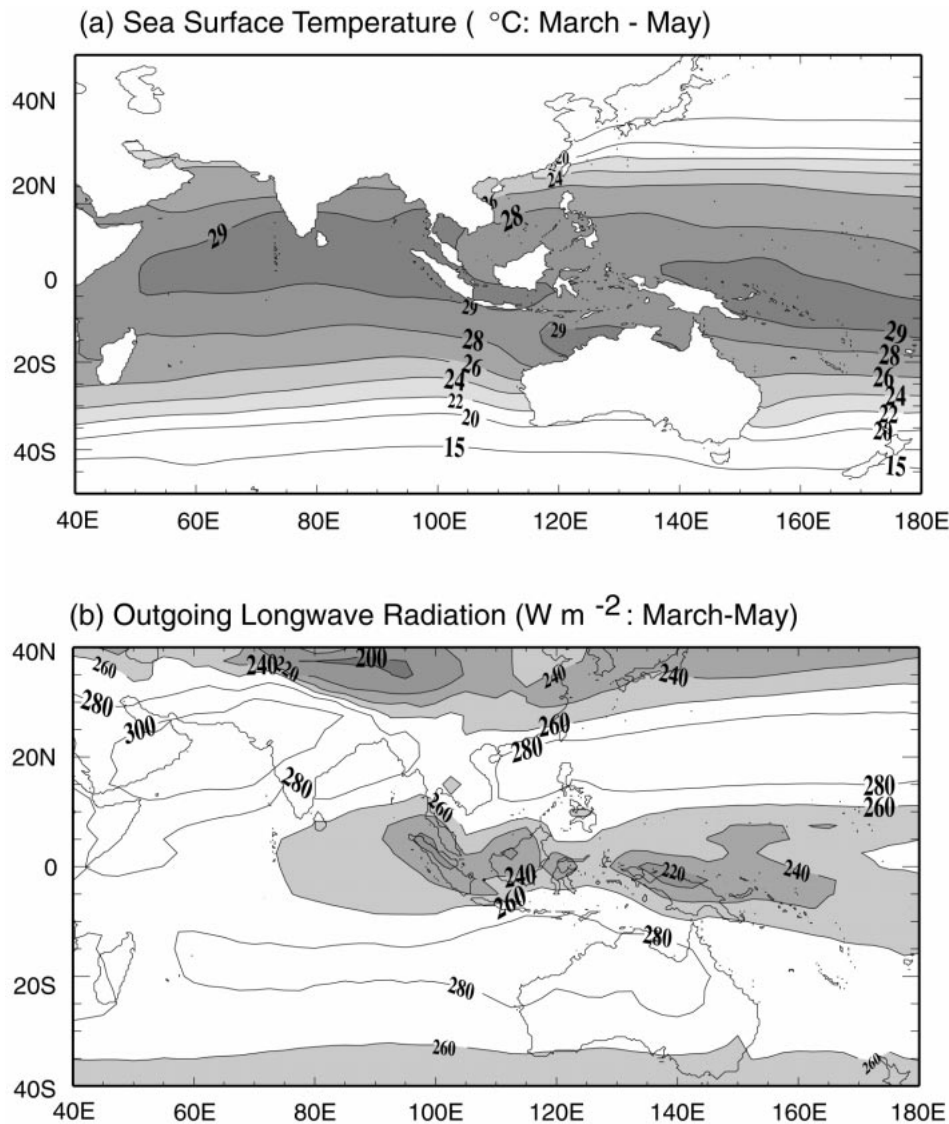E-mail: johannes@soest.hawaii.edu

FIG. 1. Mean climate of the Indian Ocean and the tropical western Pacific Ocean for (a) the SST (°C) and (b) the outgoing longwave radiation (OLR: W m^{-2}) measured from satellite.

predictability (WCRP 1985). A fundamental aim of TOGA was to understand the basic physical processes that determine the heat and energy balances of the warm pool as it had become clear that advances in the prediction of ENSO would require a detailed modeling of warm pool processes. The TOGA Coupled Ocean–Atmosphere Response Experiment (TOGA COARE; Webster and Lukas 1992) was organized with the specific aim of understanding the heat budget of the Pacific Ocean warm pool.

The objective of the Central Equatorial Pacific Experiment (CEPEX 1993) was to study the so-called thermostat hypothesis of Ramanathan and Collins (1991) that addressed directly the question of how the Pacific Ocean warm pool temperature stayed within narrow bounds (Fig. 2a). The hypothesis proposed that warm SST enhances local convective activity that, through the

increase of upper-tropospheric cloud cover, reduces the solar radiation flux at the surface, allowing the ocean to cool. The now cooler SST reduces cloudiness (presumably through decreasing convective instability), allowing an increase in insolation and subsequently warmer SSTs, and so on. However, a number of studies (e.g., Fu et al. 1992; Stephens and Slingo 1992; Wallace 1992; Hartmann and Michelsen 1993) suggest that processes associated with atmospheric motions caused by the thermodynamical imbalances are also important in regulating SST. Thus, in the Pacific Ocean the enhanced evaporation and ocean mixing caused by the atmospheric circulation play a critical role in regulating SST. More recent studies have substantiated the joint role of atmospheric dynamics in regulating warm pool SST (e.g., Lau and Sui 1997; Fasullo and Webster 1999).
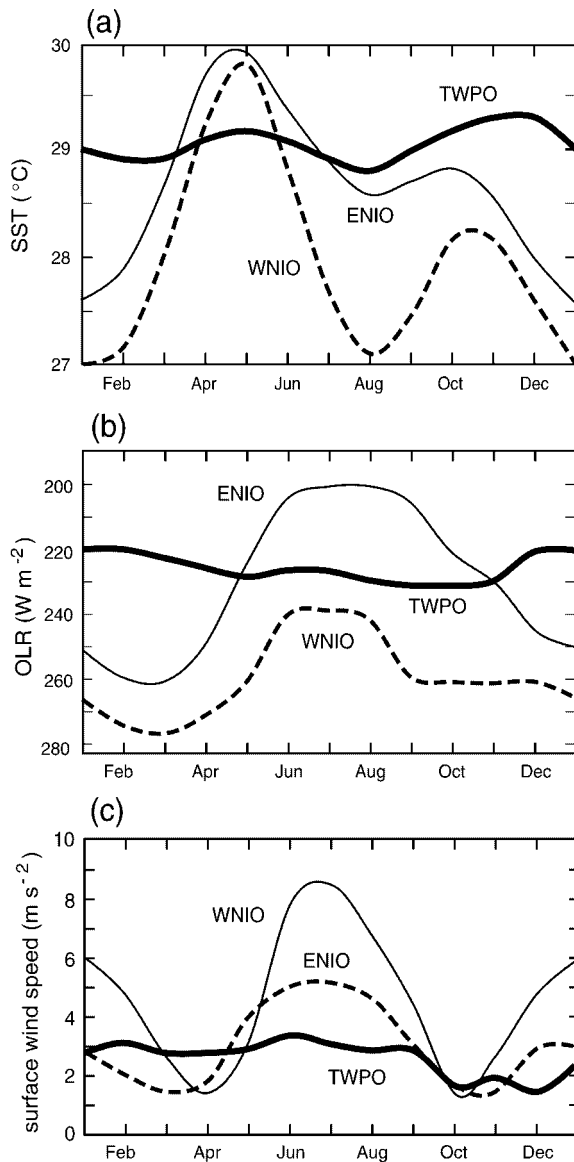
FIG. 2. Annual cycles of the mean monthly (a) SST (°C), (b) OLR (W m^{-2}: ordinate scale reversed), and (c) surface wind speed (m s^{-1}) for the tropical western Pacific Ocean (TWPO: 10°S–10°N, 140°–180°E), the northeastern Indian Ocean (ENIO: equator–20°N, 80°–105°E), and the northwestern Indian Ocean (ENIO: equator–20°N, 40°–80°E).

The investigations described above have concentrated on the SST regulation in the Pacific Ocean. However, the SST distribution in the Indian Ocean is also important in determining the strength of the Asian monsoon, as suggested by a number of recent diagnostic studies (e.g., Hastenrath 1987; Harzallah and Sadourny 1997; Sadhuram 1997; and Clark et al. 2000). Part of the Indian Ocean SST variability appears to be associated with ENSO (Torrence and Webster 1999), but there also appears to be variability that is endemic to the Indian Ocean itself (Meehl 1987, 1997; Webster et

al. 1999). Thus, we investigate the processes that regulate the heat balance of the Indian Ocean and, in particular, the amplitude of the annual cycle of the SST.

The processes proposed to regulate the SST in the western Pacific Ocean are inadequate to explain completely the evolution of SST in the tropical Indian Ocean. The simplest way to illustrate these inadequacies is to compare the climatologies of SST and convection in the two tropical warm pools (Figs. 1–3). The comparison yields some similarities but also major differences:

1) Both warm pools have long-term mean SSTs that are in excess of 29°–30°C (Fig. 1a). The western Pacific Ocean remains within this small SST range for the entire year (Fig. 2a), although the location of the SST maximum migrates north and south about the equator following the locus of maximum insolation, albeit lagging by 2–3 months. The annual cycle of the northern Indian Ocean SST (Fig. 2a) possesses a slightly larger range. The mean SST of the Indian Ocean between the equator and 20°N falls to about 27°C, although in the equatorial regions (10°N to 10°S) the mean SST remains greater than 28°C for the entire year. During the boreal spring and early summer, the northern Indian Ocean becomes the warmest body of open water in the Tropics exceeding the mean tropical western Pacific temperature by 1°C. After the onset of the South Asian summer monsoon, the North Indian Ocean cools (Fig. 2a) as a result of strong coastal upwelling and enhanced evaporation (e.g., Knox 1986).

2) Long-term mean warm SSTs in the western Pacific Ocean are collocated with large values of mean atmospheric convection (signified by low values of OLR; Arkin and Meisner 1987) during most of the year (Figs. 2a,b). On the other hand, the northern Indian Ocean is singular in its lack of deep convection (high values of OLR) in spring and early summer during its warmest phase (Figs. 1b and 2a,b).

3) Figure 3 shows relationships between mean monthly SST and OLR in the regions of the two warm pools indicated in the bottom panels for the boreal spring period. The SST–OLR pairings show a fairly strong linear relationship in the Pacific Ocean (Fig. 3a) with the depth of convection (colder OLR) increasing with increasing SST. This SST–OLR relationship in the Pacific Ocean provided the fundamental observation for Ramanathan and Collins (1991) in their original posing of the thermostat hypothesis. On the other hand, the SST–OLR pairings for the Indian Ocean show an absence of correlation (Fig. 3b,c). Figures 3b,c display SST–OLR pairings of both the western and eastern Indian Ocean regions to illustrate the fact that the eastern Indian Ocean is similar to the western Indian Ocean but dissimilar to the Pacific.

4) Mean surface wind fields are generally light over the Pacific warm pool for most of the year and over the

TABLE 1. Comparison of the surface energy balance for the western Pacific Ocean (WPO: 10°N–10°S, 130°E–180°) and the northern Indian Ocean (NIO) north of 0°N. Values are given for the NIO east of 80°E (E) and west of 80°E (W). Data based on COADS from Oberhuber (1988) have been used. Wind speed values have been rounded to the nearest meter per second and flux values to the nearest 5 W m^{-2}. Values are shown for winter, Dec–Feb; spring, Mar–May; summer, Jun–Aug; and autumn, Sep–Nov.

| Quantity | WPO | | | | NIO | | | | | | | |
| | | | | | Winter | | Spring | | Summer | | Autumn | |
	Winter	Spring	Summer	Autumn	W	E	W	E	W	E	W	E
Mean surface wind speed (m s^{-1})	4	4	4	4	7	4	4	3	11	8	4	3
Net solar flux (W m^{-2})	165	160	150	170	180	170	230	200	190	170	195	165
Net longwave flux (W m^{-2})	−45	−50	−45	−45	−65	−60	−50	−45	−40	−35	−45	−40
Latent heat flux (W m^{-2})	−100	−80	−90	−90	−140	−100	−85	−65	−130	−120	−90	−80
Sensible heat flux (W m^{-2})	−5	−5	−5	−5	−5	−5	0	0	0	0	0	0
Net heat flux into ocean (W m^{-2})	15	25	10	30	−30	5	95	90	20	15	60	45

Indian Ocean before the monsoon onset (Fig. 2c). Stronger winds occur in the equatorial eastern Indian Ocean and the western Pacific Ocean during the boreal winter and spring, associated with convective mesoscale clusters and/or westerly wind bursts. However, these are episodic and short-lived events compared to the averaging period and the mean winds remain very light (Fasullo and Webster 2000).

From the above discussion, it is clear that the simple radiative–convective SST feedbacks posed for the Pacific Ocean by Ramanathan and Collins (1991) almost certainly do not dominate in the Indian Ocean. At this stage, one cannot rule out the possibility that the atmospheric circulation–radiative feedback processes posed by Hartmann and Michelson (1993) or Stephens and Slingo (1993) for the Pacific Ocean, are not equally operative in the Indian Ocean. However, in the next section we will show that this is likely not the case. In this study we test the hypothesis that horizontal oceanic

advections of heat are of essential importance in the annual cycle of the heat balance and SST of the Indian Ocean.

In the next section, we examine the surface energy budgets of the Indian and Pacific Ocean warm pools. In section 3 we use a dynamic ocean model to study the annual cycle and the SST evolution in the Indian Ocean. Section 4 discusses the interannual variability of the North Indian Ocean. A regulatory model of the annual cycle of the coupled ocean–atmosphere–land monsoon system is introduced in section 5. Some conclusions are made in section 6.

2. A comparison of warm pool surface energy balances

Through TOGA COARE, the surface heat balance in the western Pacific Ocean is fairly well known (Godfrey et al. 1998), much more so than that of the Indian Ocean.
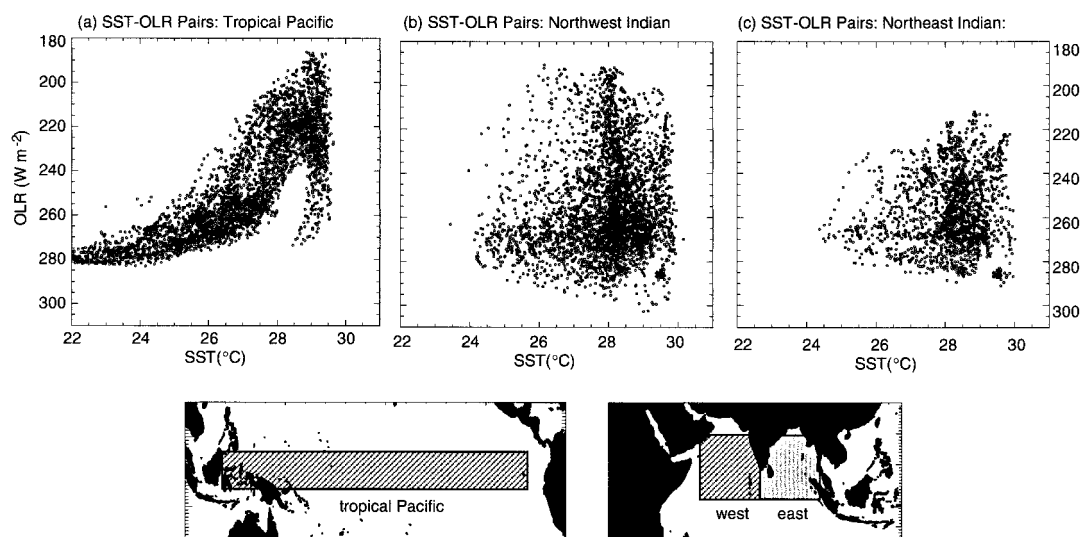

FIG. 3. OLR–SST (W m^{-2} and °C with ordinate scale reversed) pairs for (a) the tropical Pacific Ocean in the region 5°S–5°N, 120°E–90°W, (b) the northern Indian Ocean for the region equator–20°N, 55°–80°E, and (c) the northern Indian Ocean, equator–20°N, 80°–100°E. The geographical areas are depicted by the areas within the shaded boxes on map panel. Mean monthly values are plotted for Mar, Apr, and May for all points in the boxes. Data are from 1972–89.

TABLE 2. Comparison of the observed vs computed SST changes for the western Pacific Ocean (WPO: 10°N–10°S, 130°E–180°) and the northern Indian Ocean (NIO) north of 0°N. Data based on COADS from Oberhuber (1988) have been used. Computations are made using the one-dimensional ocean mixed layer model of Kantha and Clayson (1994). Values are shown for winter, Dec–Feb; spring, Mar–May; summer, Jun–Aug; and autumn, Sep–Nov. Units are °C (3 month)$^{-1}$.

	WPO				NIO			
	Winter	Spring	Summer	Autumn	Winter	Spring	Summer	Autumn
Computed	1	1	1	1	−2	12	−3	2
Observed	−0.5	+0.3	−0.25	+0.5	0	2	−2	1

Most estimates of the Indian Ocean (e.g., Oberhuber 1988) depend on datasets compiled from ships of opportunity as well as other surface and subsurface data collected some decades ago (e.g., Hastenrath and Greischar 1989, 1993). Table 1 lists the best estimates of the components of the surface energy budget from data for the two regions (Oberhuber 1988; TOGA COARE International Project Office 1994; Webster et al. 1996; Godfrey et al. 1998) for the boreal summer and winter. Seasonal averages are shown for the Indian Ocean north of the equator for the eastern (east of 80°E) and western (west of 80°E) regions, and for the tropical western Pacific between 10°N and 10°S and from 130°E to 180°. The most striking difference between the Indian and Pacific Oceans is the much greater solar flux into the ocean in the northern Indian Ocean for most of the spring and early summer when 24-h period means reach 230 W m^{-2}, compared to 150 W m^{-2} for the western Pacific. Overall, the net heat budget in the Pacific Ocean warm pool is nearly in balance, with a net heat flux between 10 and 20 W m^{-2} into the ocean (Godfrey et al. 1998). However, in the North Indian Ocean during the March–May period, the net flux is in the range 75–100 W m^{-2}, principally because of the large solar radiation flux associated with the absence of clouds (Oberhuber 1988).[1] During the boreal winter, the North Indian Ocean surface energy balance becomes negative approaching −30 W m^{-2} in the west.[2]

To estimate the variation of SST due purely to thermodynamical forcing and vertical ocean mixing in each of these regions, we use the one-dimensional ocean mixed layer model developed by Kantha and Clayson

(1994). Calculations are carried out to a depth of 200 m using a vertical resolution of 1 m. The model was initialized using data from Levitus (1982). The model assumes that there is no horizontal advection and therefore provides the change in SST due to surface fluxes alone or to mixing with cooler subthermocline water. The results of the calculations may be thought of as the heat balance of an entire warm pool if it assumed that there is no oceanic horizontal flux of heat into or out of the warm pool. The forcing functions of the model are the climatology listed in Table 1. A more comprehensive analysis using the Kantha–Clayson model is given by Webster (1994).

Table 2 shows a comparison between the observed and modeled SST changes. The mixed layer model shows a small warming and cooling of SST averaging about +0.3°C month^{-1} for the Pacific Ocean warm pool, which is about a factor of 2 greater than observed (Fig. 2a). However, the modeled SST changes for the northern Indian Ocean are about +4°C month^{-1} during the spring and early summer, which is a factor of 3 or 4 larger than observed. By extrapolation, if no other processes are taken into account (e.g., horizontal advection of heat, upwelling of cool subsurface water), the northern Indian Ocean SST should warm by about 12°C during spring and early summer before the onset of the summer monsoon. Also, the model suggests a cooling of order 1°C month^{-1} during the winter.

The problem is to account for an upper ocean heating (or cooling) rate that is much smaller in the North Indian Ocean than the theoretical thermodynamical limit deduced using the Kantha–Clayson model. An explanation of the difference is necessary because the high springtime solar radiation (Table 1) is not offset by the generation of highly reflecting cloud as SST increases, as would be necessary to be in accord with the Ramanathan and Collins (1991) hypothesis. In fact, Fig. 2b shows an OLR maximum (minimum convection) in the northern Indian Ocean during the boreal spring. Nor is it likely that enhanced evaporation and the atmospheric transport of heat away from the northern Indian Ocean can explain the differences between observations and theory. Oberhuber (1988) estimates the evaporation in the North Indian Ocean to be between 65 and 85 W m^{-2} (Table 1). Evaporation would have to be greater than 180 W m^{-2} to balance the heat budget. With all other factors held constant, the wind speed would have to be

[1] Recent observations taken during May 1999 in the Bay of Bengal during the Joint Air–Sea Monsoon Interaction Experiment (JASMINE) corroborated Oberhuber's (1988) estimates. Data courtesy of C. Fairall Environmental Technology Laboratory/National Oceanic and Atmospheric Administration and F. Bradley Commonwealth Scientific and Industrial Research Organisation Australia).

[2] In this paper, we concentrate on the Indian Ocean north of the equator. However, the surface flux into the Indian Ocean region between the equator and 20°S tends to be opposite in sign to the values north of the equator. Using the data from Oberhuber (1988) net heat fluxes into the 0°–20°S zonal strip are +60, +15, −65, and +20 W m^{-2} for the boreal winter, spring, summer, and fall, respectively. These values are consistent with the earlier climatologies (e.g., Hastenrath and Lamb 1979a,b; Hastenrath and Greischar 1989).
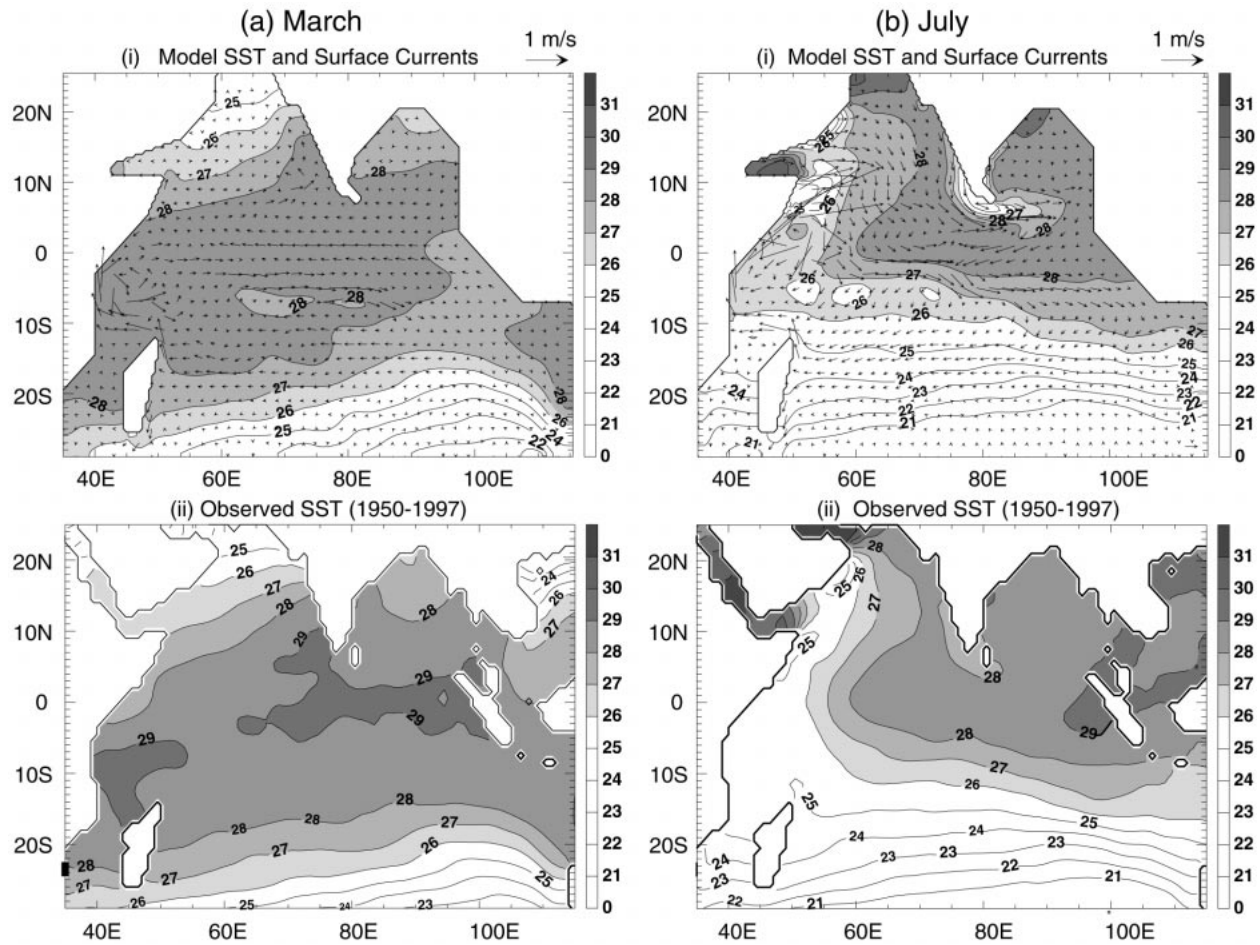
FIG. 4. Mean model T_m (°C) and current vectors for layer 1, and climatological SST for Mar for 1950–97 using the GISST dataset (Rayner et al. 1996) for (a) Mar and (b) Jul.

greater than 15 m s^{-1} during the boreal spring, which is almost a factor of 5 greater than climatology. Similarly, in winter, evaporation would have to decrease by half the climatological value to account for the difference. By the process of elimination, only an oceanic transport of heat into or out of the North Indian Ocean can account for the observed SST trends in the North Indian Ocean.

3. Oceanic regulation of SST in the northern Indian Ocean

To test the hypothesis that ocean heat transports regulate SST in the Indian Ocean, we use the McCreary et al. (1993) 2½ layer dynamic upper-ocean model.[3] Although there is little subsurface data in the Indian

Ocean with which to evaluate model results,[4] the model appears to replicate what is known about the mean annual surface structure of the Indian ocean (McCreary et al. 1993). Except where otherwise specified, atmospheric forcing of the ocean is prescribed from monthly climatological data of Oberhuber (1988).

a. Mean seasonal SSTs and surface currents

The simulated mean upper-layer temperature, T_m, and current vectors, as well as the observed mean SST, for March and July, are shown in Figs. 4a and 4b. For March (Fig. 4a), the model develops slightly cooler SSTs in both the equatorial region south of India and the area north of Madagascar, reaching only 28°C instead of the

---

[3] Details of the model are given in the appendix together with model terminology.

[4] Atlases of climatological Indian Ocean surface and subsurface fields (the latter computed as residuals of surface values) by Hastenrath and Lamb (1979a,b) and Hastenrath and Greischar (1989, 1993) provide syntheses of the data available for the region.

observed 29°C. Otherwise, the basic spatial structure of the observed SST field is well reproduced, with the temperature gradients in both the Arabian Sea and the southern Indian Ocean being captured. A comparison of the July observed and simulated results (Fig. 4b) shows similar correspondence except for cooler SSTs off the southern tip of India that are about 2°C less than observed. The Somalia upwelling is reasonably well simulated in the model, although the model temperatures are about 1°C warmer than observed along the equatorial East African coast. In summary, the 2½ layer model simulates mean structures in the Indian Ocean sufficiently well to allow it to be used as the principal analytic tool for the study.

b. Annual cycle of the heat balance of the northern Indian Ocean

The northward heat flux between two positions along a line of constant latitude is defined by

$$Q_v(t) = \rho C_p \iint vT \, dx \, dz, \tag{1}$$

where $v(x, z, t)$ and $T(x, z, t)$ are the meridional velocity and temperature, respectively. Longitude and depth are denoted by x and z, respectively. In the present analysis, the meridional velocities and temperatures used are v_i and T_i, respectively, where i represents the model layer ($i = 1, 2$). In this calculation $T_{i=1}$ is the mass-weighted average of T_m and T_f, the mixed layer and fossil layer temperatures (see appendix). Integrals in longitude are evaluated from the western to eastern boundaries of the Indian Ocean, and integrals in depth are computed through the individual layers, h_i. For the 2½ layer model, it is possible that the volume integral of the mass analyzed for heat budget calculations in not constant in time within the upper 2 layers. With this in mind, the heat transport was calculated assuming mass conservation in the bottom layer, with infinite depth, zero currents, and finite mass transport. This procedure allows the calculation of true heat transport as opposed to mass transport, as discussed by Hall and Bryden (1982). The bottom layer volume transport is defined as

$$\int v_3 H_3 \, dx = -\int (v_1 H_1 + v_2 H_2) \, dx \tag{2}$$

with the dynamically active layers 1 and 2 overlying the deep layer 3. With layer temperatures T_i ($i = 1$ to 3), the total heat transport then becomes

$$Q_v = \rho C_p \int (v_1 H_1 T_1 + v_2 H_2 T_2 + v_3 H_3 T_3) \, dx$$
$$= \rho C_p \int [v_1 H_1 (T_1 - T_3) + v_2 H_2 (T_2 - T_3)] \, dx. \tag{3}$$

The deep ocean temperature (T_3) was taken as 4°C after Levitus (1982). Differences using the mass conservation method versus having no balancing flow in the deep layer were very small. However, all results shown use the mass conservation method.

The rate of heat storage, Q_t, and the net surface heat flux, Q_s, are defined as

$$Q_t(t) = \rho C_p \iiint \frac{\partial T_i}{\partial t} \, dx \, dy \, dz \quad \text{and} \tag{4}$$

$$Q_s(t) = \iint (Q_{sw} + Q_{lw} + Q_{le} + Q_{sh}) \, dx \, dy, \tag{5}$$

respectively. The four terms in the integrand of (5) represent the surface fluxes of heat due to shortwave radiation, net longwave radiation, and latent and sensible transfer, respectively. To compute the heat storage, integration with depth was carried out to 500 m, which is below the depth of the lower active of the model (layer 2), thus ensuring a constant volume for the analysis.

Figure 5a shows the northward oceanic heat transport across the equator as a function of time of year [from Eq. (3)], together with the evolution of the net surface heat flux over the ocean basin north of the equator [from Eq. (5)] and the heat storage of the uppermost ocean layers for the same region [Eq. (4)]. Essentially, the major balances of heat in the North Indian Ocean are between the transport and storage terms. For the heat budget to be balanced for a closed region such as the North Indian Ocean, transport into the region plus surface flux into the surface, must equal the net heat storage within the closed region. That is, $Q_v + Q_s = Q_t$. Therefore, during periods of low surface heat flux, the major balance is approximately $Q_v = Q_t$. A moderate southward transport of heat (negative Q_v) is found during the spring, increasing in magnitude by early summer. The heat flux reverses during the winter when the North Indian Ocean is losing considerable amounts of heat by strong wind evaporation and mixing (see Table 1). Figure 5b shows that the net heat transport across the equator consists of opposing flows in the upper and lower layer of the model between May and October. Between November and April the fluxes in the two layers are both northward. The reversal of the values of heat transport between summer and winter may be thought of as a seasonally reversing meridional circulation cell, as described by McCreary et al. (1993) and Wacongne and Pacanowski (1996). The net southward cross-equatorial heat transport during the spring and summer months compensates for the excess surface heat flux into the North Indian Ocean with peak summer values reaching 2 PW.

Figure 6 displays the seasonal breakdown of the components of the heat balance of the North Indian Ocean. Seasonal mean fluxes and transports are depicted as arrows. For the spring months (March–May), the strong net surface flux into the North Indian Ocean (+0.51

(a) North Indian Ocean heat balance

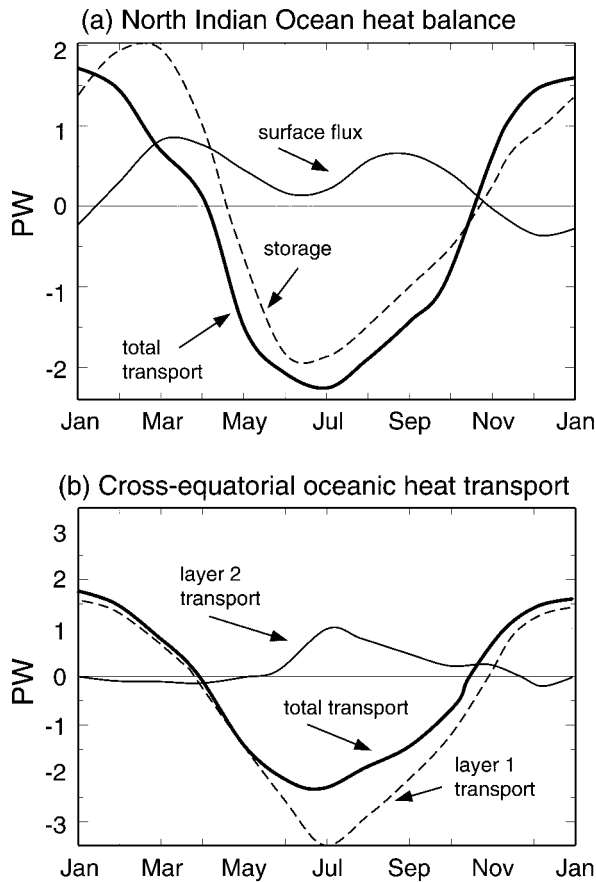(b) Cross-equatorial oceanic heat transport

FIG. 5. (a) Annual cycle of the heat balance calculated with the 2½ layer model for the Indian Ocean basin north of the equator. Model was forced by an observed annual cycle of COADS winds and surface radiation fluxes. Storage is defined as the time rate of change of heat content of the upper ocean layers in the North Indian Ocean. Transport refers to the net heat flux across the equator with positive values indicating a net heat gain or northward transport across the equator, while negative values indicate net heat loss or southward transport across the equator. Values are given in petawatts (1 PW = 10¹⁵ W). (b) The annual cycle of the cross-equatorial transport for each of the two active layers of the model.
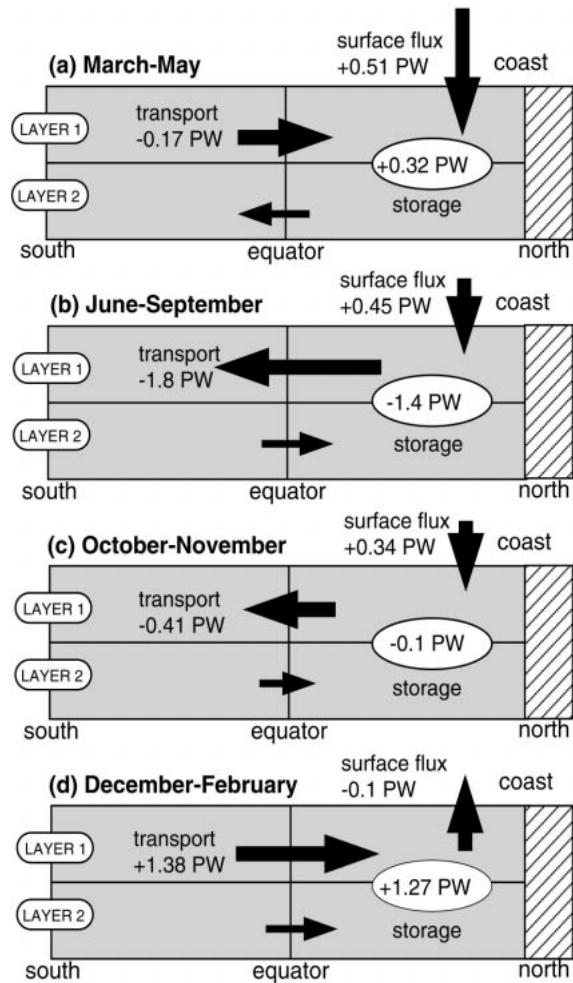

FIG. 6. Schematics of the seasonal mean heat balance of the Indian Ocean Basin north of the equator for the periods (a) spring (Mar–May), (b) summer (Jun–Sep), (c) autumn (Oct–Nov), and (d) winter (Dec–Feb). Arrows (scaled for magnitude) denote the directions of the cross-equatorial fluxes in each layer. The values of transport and storage displayed in the figures are the sums of both model layers. Units: PW.

PW) is balanced by a moderate increase in heat storage in the upper ocean north of the equator (+0.32 PW), as well as by smaller southward mean heat transport (−0.17 PW). During the summer monsoon months (June–September), the net surface heat flux in the North Indian Ocean is still into the ocean (+0.45 PW), but the major heat balance occurs between the very strong southward heat transport (−1.8 PW) and decreases in heat storage (−1.4 PW). The situation reverses in the boreal winter (December–February) as weak net surface cooling (−0.1 PW) is more than compensated by net northward heat transport (+1.38 PW) and increases in heat storage (+1.27 PW).

In both spring (March–May) and autumn (October–November) the net cross-equatorial fluxes are weak compared to values in summer and winter. Noting the annual cycle in Fig. 5a, it can be seen that the weak

transports result from the change of sign in the transport. In March the mean transport is 0.7 PW, but in May the value is −1.6 PW, contributing to a mean transport of only −0.17 PW. Similarly, in October the oceanic transport is −1 PW, but in November it is 1.2 PW, resulting in a weak northward flux. Thus, spring and autumn are transition seasons in terms of northward ocean heat transports with the changes occurring more rapidly than at any other time of the year.

Recent studies using a variety of models, ranging from Indian Ocean Basin models to ocean general circulation models (Wacongne and Pacanowski 1996; Gartenicht and Schott 1997; Lee and Marotzke 1997), have also found similar magnitudes in the seasonally reversing meridional heat transport with annual mean cross-equatorial heat transport values in the range of −0.2 to
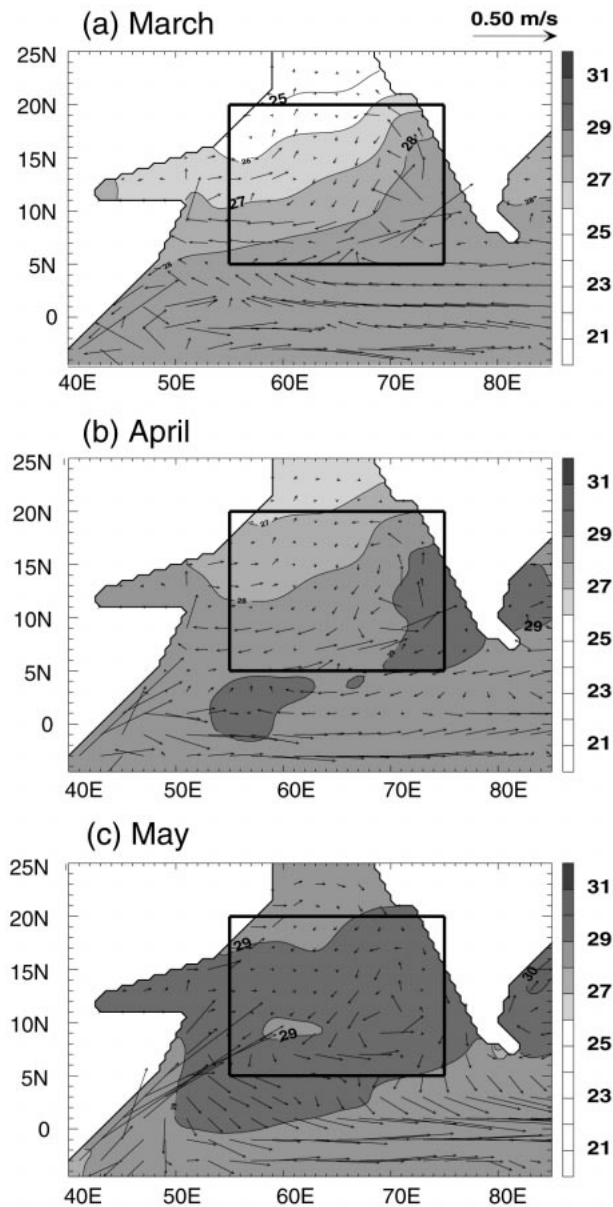
FIG. 7. Mean model T_m (°C) for (a) Mar, (b) Apr, and (c) May, for the northwestern section of the model basin with current vectors for layer 1 overlaid. Region in which computations were made is boxed.
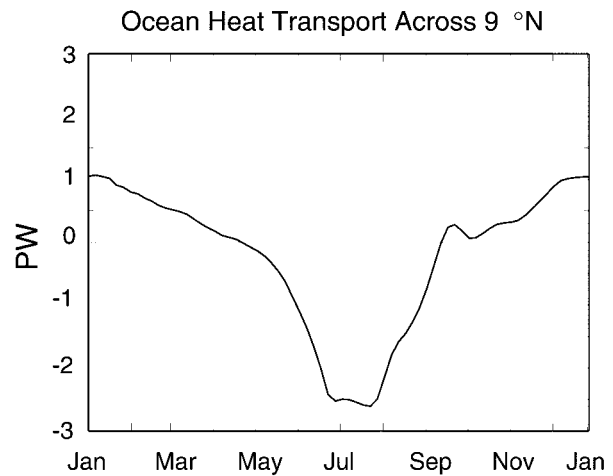

FIG. 8. Total heat transport across 9°N between the Somalia and Indian coasts as a function of time of year. Units: PW.

sequent simulation discussed in the paper. However, as the major heat flux from the throughflow is into the South Indian Ocean (Hirst and Godfrey 1993; Godfrey 1996), this may not be a critical omission for the study of the North Indian Ocean heat balance.

c. Advective processes

To examine more closely the role of advective processes controlling SST in the northern Indian Ocean, we focus on the region 5°–20°N and 55°–75°E. Figures 7a–c show model upper-layer temperature and current vectors in the northwest Indian Ocean for March, April, and May, respectively. In March (Fig. 7a) there is a temperature gradient from the northwest to the southeast corners of the box of about 2.5°C (2000 km)$^{-1}$. For upper-ocean heat advection to account for the 3–4°C month^{-1} cooling in the northern Indian Ocean, there would need to be a component of the surface currents in the direction of the SST gradient of about 60 cm s^{-1}. Throughout the spring months, the model currents in layer 1 in the central Arabian Sea are on the order of between 5 and 20 cm s^{-1} in a south-southeasterly direction with compensating northerly layer 1 flows on the Indian and Somali coasts with magnitudes of 10–30 cm s^{-1} and 30–80 cm s^{-1}, respectively. During March (Fig. 7a), currents in the interior Arabian Sea are generally southward between 5 and 15 cm s^{-1} with northward currents at the boundaries of between 20 and 30 cm s^{-1}. In April (Fig. 7b), interior currents are roughly the same order of magnitude as earlier but with slightly weaker boundary currents. In May (Fig. 7c), as the SST gradient reduces, the currents strengthen both in the interior (10–20 cm s^{-1}) and at the boundaries (20–60 cm s^{-1}).

The resulting effect of the model currents relative to the SST gradients are shown in Fig. 8, which displays the heat transport in both model layers computed using
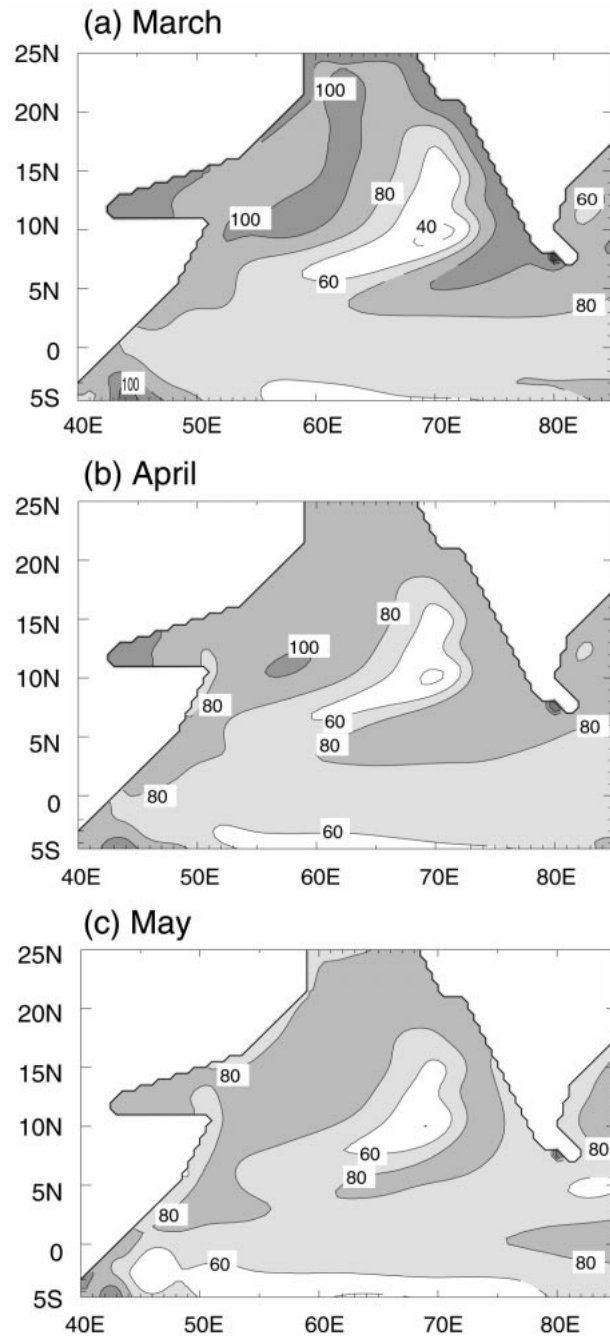
−0.4 PW. However, there are two issues that need to be noted.

1) The heat flux distributions shown in Figs. 5 and 6 are long-term averages and result from the use of long-term atmospheric forcing. In subsequent sections we will show that there is both interannual variability in the fluxes, storages, and heat transports (Fig. 12) and that within one season there is a strong intraseasonal component to the heat transports across the equator.

2) The Indonesian throughflow has not been included in the simulations described above, nor in any sub-

(a) March

(b) April

(c) May

FIG. 9. Mean layer-1 depths (m) for (a) Mar, (b) Apr, and (c) May for the northwest section of the Indian Ocean.

Entrainment Velocity

FIG. 10. Annual cycle of the entrainment velocity (cm day^{-1}) between model layers 1 and 2 for the region 5°–20°N, 55°–75°E.

SST between June and August. However, it does not completely explain the lack of the very large SST increases in the far North Indian Ocean during the boreal spring. It is possible that changes in layer depths and entrainment also influence the development of SST fields during this period. Figures 9a–c show the depth of the upper model layer for March, April, and May, respectively. Layer 1 depths shallow by about 20 m over the Arabian Sea over the 3-month period. Such shallowing is not inconsistent with mixing of cooler water into the upper layer from the deeper ocean or with the thermal stabilization in the low wind–high insolation regime (Tomzak and Godfrey 1994). Figure 10 displays the entrainment velocity (w_e as defined in the appendix) between model layers 1 and 2 over the area 5°–20°N, 55°–75°E as a function of time of year. The period of March–May shows substantial negative entrainment velocities that detrain warmer upper-layer water into the cooler lower layer consistent with the thinning of the upper layer. The summertime peak in positive values of w_e during late July and early August in Fig. 10 results from large increases in layer 1 depths near the Somali coast, due to strong Ekman pumping in the region of the Great Whirl.

d. Dynamic components of heat transport

The heat transport can be broken down into two major components: the wind-driven Ekman component and the geostrophic component. Following Levitus (1987), the Ekman component of the heat transport is given by

$$Q_{v(EK)} = C_p \int \frac{-\tau^x}{f}(T_s - [T]) \, dx, \qquad (6)$$

where T_s denotes the temperature at the ocean surface, $[T]$ is the vertically averaged temperature (or a deep reference temperature) of the return flow, τ^x is the zonal wind stress, and f is the Coriolis parameter. The zonal wind stress is derived from the climatological Comprehensive Ocean–Atmosphere Data Set (COADS) data used to force the model. Here T_m was used as the temperature for T_s, and a linear interpolation between T_2

(3) along 9°N between the Somali and Indian coasts as a function of time of year. Although the net heat transport is small and to the north for March and early April, the sign of the heat transport reverses in mid-April, becoming strong and to the south by early June.

The strong southward heat transport in the peak summer months, noted above, provides a clue to the reason why there is a sharp decrease in North Indian Ocean
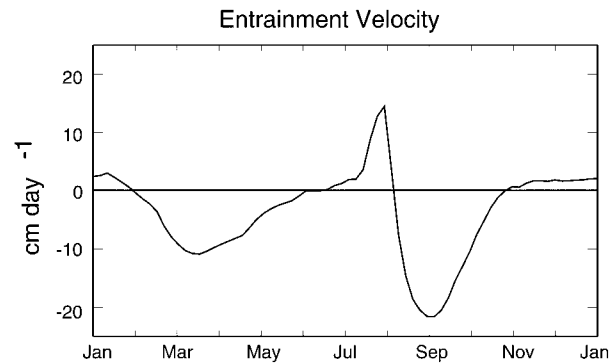
and T_3 (the temperature of the deep inert layer) was used for the temperature of the return flow, so as to represent the vertically averaged temperature [T]. Levitus (1987) notes that because tropical surface temperatures are generally greater than 20°C, errors of 1°C in the vertically averaged temperature used to calculate the return flow, result in only small errors in the heat transport. Thus, errors resulting from a miscalculation of the return flow temperature should be small here as well.

Calculation of the geostrophic component requires using the ''direct method'' described by Boning and Bryan (1996). This method involves splitting the variables of v and T into their depth-averaged parts and their deviations from the depth average such that $v = [v] + \hat{v}$ and $T = [T] + \hat{T}$, resulting in

$$Q_v = \rho C_p \left\{ \int D[v][T]\, dx + \iint \hat{v}\hat{T}\, dx\, dz \right\}, \quad (7)$$

where D is the depth of the ocean. The terms on the right-hand side of (7) represent the barotropic and baroclinic parts of the heat transport, respectively. As there is no barotropic component in the ocean model, the total transport in the model [$Q_{v(\text{TOT})}$] may be considered to be baroclinic. The baroclinic heat transport can be thought of as being comprised of the contributions from the Ekman transports at the surface $Q_{v(\text{EK})}$, and the contribution of the geostrophic flow in the ocean interior $Q_{v(G)}$. The geostrophic component can then be derived as

$$Q_{v(G)} = Q_{v(\text{TOT})} - Q_{v(\text{EK})}, \quad (8)$$

where $Q_{v(\text{TOT})}$ is the total heat transport as described by (3), but for the interior ocean only (i.e., farther than 3° longitude from any boundary) so as to allow for a proper comparison to the interior Ekman transport. The geostrophic flow results from meridional variations in layer depths and layer temperatures, which, collectively, generate density gradients and pressure forces.

Figure 11 shows the zonally integrated values for each of these components of Q_v [as given in Eqs. (6) and (8)] plotted as a function of latitude for the northern Indian Ocean, and for the period April–May. As balances in the Ekman theory break down as one approaches the equator, values for $Q_{v(\text{EK})}$ and $Q_{v(G)}$ are shown only for regions north of 4°N. Figure 11 shows that for the northern Indian Ocean in the late spring and early summer, it is the Ekman, or the wind-driven component of the heat transport, that is the major contributor of transport south of 10°N. Between 11° and 14°N, the geostrophic component provides a northward transport, balancing the southward Ekman component and producing a small net southward transport.

4. Interannual variability of the heat balance of the North Indian Ocean

Multiyear integrations were compiled using 5-day mean data from 1984 to 1990 using National Centers
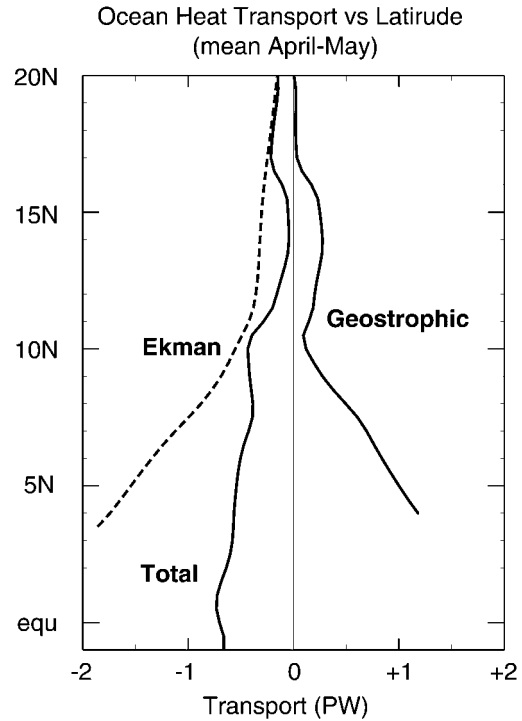

FIG. 11. Average values for Apr and May of the components of the total heat transport [$Q_{v(\text{TOT})}$, $Q_{v(\text{EK})}$, and $Q_{v(G)}$] as a function of latitude. Units: PW.

for Environmental Prediction–National Center for Atmospheric Research (NCEP–NCAR) reanalysis data (Kalnay et al. 1996) for winds, air temperature, and surface specific humidity, and the International Satellite Cloud Climatology Program (ISCCP) satellite-derived net surface shortwave dataset of Bishop and Rossow (1991). The results of the integrations for years 1984–90 are shown in Figs. 12a,b. Figure 12a shows the complete time series of net surface flux into the North Indian Ocean, the storage, and the cross-equatorial advection of heat. Figure 12b shows the annual averaged values of the same quantities.

In most years there is a general balance between cross-equatorial transport of heat and the net flux into the northern Indian Ocean, as found with the climatological annual cycle shown in Fig. 5. However, there is also considerable interannual variability particularly in the years 1987 and 1988. These years are interesting as they represent, respectively, substantially weak and strong years of the south Asian monsoon, as well as the El Niño and La Niña phases of the ENSO cycle (Webster and Yang 1992). During these years the modeled heat balance of the North Indian Ocean is quite different from the average annual cycle. Annually integrated values, as seen in Fig. 12b, show that the southward heat transport is substantially reduced in 1987, and is accompanied by an overall increase in heat storage in the northern Indian Ocean. An almost complete reversal of this situation occurs in 1988 with a much larger southward
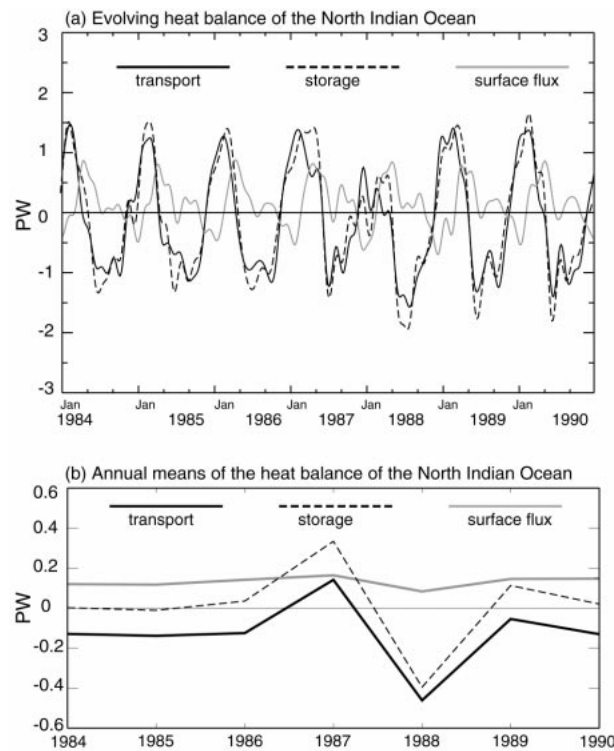
FIG. 12. (a) Heat balance of the Indian Ocean basin north of the equator for model simulations of the period 1984–90 showing the cross-equatorial heat transport, and the heat storage and surface flux of the North Indian Ocean. (b) Annually averaged values of transport, storage, and surface flux as defined in (a). Model was forced by 5-day average NCEP surface winds (Kalnay et al. 1996) and ISCCP fluxes (Bishop and Rossow 1991).

heat transport and a reduction of the net heat storage of the North Indian Ocean. In 1988, the increased transport is consistent with the increased strength of the wind-driven ocean meridional circulation cell, resulting from the stronger than average summer monsoon winds. Similarly, in 1987 the reduced cross-equatorial heat transport matches a weakened meridional cell driven by lower than average monsoon winds.

5. A regulatory model of the annual cycle of the Indian Ocean monsoon system

To this point, we have shown that there is a very strong annual cycle of cross-equatorial oceanic heat transport from the hemisphere of net positive surface flux into the hemisphere of negative net flux in the Indian Ocean. From Fig. 5 the amplitude of the transport (averaged across the entire Indian Ocean) varies between ±2 PW compared to an annual average of −0.2 PW. We have argued that these transports are responsible for the modulation of annual cycle of the SST in the northern Indian Ocean where the observed variation of the SST is much smaller than would be expected from local surface fluxes considerations alone. We now present a simple model of the modulation of the annual

cycle of the SST in the context of the coupled ocean–atmosphere system.

Consider the hypothetical situation where there is no horizontal heat advection in the ocean. During the boreal spring, for example, the large net surface heat flux into the North Indian Ocean would cause the SST to increase substantially as argued in section 2. Similarly, the negative surface heat fluxes in the southern Indian Ocean would lower the SST south of the equator. The spring-time surface flux differential across the equator would create a large cross-equatorial buoyancy gradient in the ocean mixed layer. As such a gradient is not observed in nature, it must relax in some manner. There are two plausible mechanisms that can produce the relaxation.

1) The development of a cross-equatorial thermohaline circulation that would relax the buoyancy gradient through transports of heat. However, the timescale to set up a thermohaline circulation is very slow (Gill 1982) and certainly not sufficiently rapid to cause a change of sign of the oceanic heat flux shown in Fig. 5a. Also, relaxation by a thermohaline circulation would not explain why the change in sign of the cross-equatorial heat transport during the spring (i.e., northward to southward: Fig. 5) coincides with the change in the direction of the atmospheric monsoonal flow.

2) The development of a wind-driven ocean heat transport across the equator. This hypothesis is consistent with the conclusion of Gartenicht and Schott (1997) that annually averaged transhemispheric oceanic heat transport is wind driven. The wind-driven transport mechanism would also explain why the sign of the heat transport changes at the same time as the monsoon wind reversal. For the cross-equatorial buoyancy gradient to be relaxed by a wind-driven circulation, the cross-equatorial transports of heat must be in the opposite direction to the meridional component of the monsoon wind field. That is, when the monsoon flow is from the Southern Hemisphere to the Northern Hemisphere (e.g., late boreal spring and summer), the wind-driven oceanic transport of heat would have be to the south. During winter, when the meridional component of the monsoon is toward the south, the oceanic heat flux would have to be to the north.

Figure 13 presents a schematic representation of how the monsoonal atmospheric flow, responding to body forces induced by cross-equatorial heating differences, drives cross-equatorial ocean heat transports from the summer to the winter hemispheres. Consider the Northern Hemisphere spring and summer (Fig. 13a), where relative heating occurs over the land areas and ocean regions of the Northern Hemisphere, and relative cooling occurs to the south of the equator. Such a meridional heating gradient (together with orographic and heating influences from Africa) drives a cross-equatorial monsoon wind gyre (e.g., Webster 1987; Webster et al. 1998)
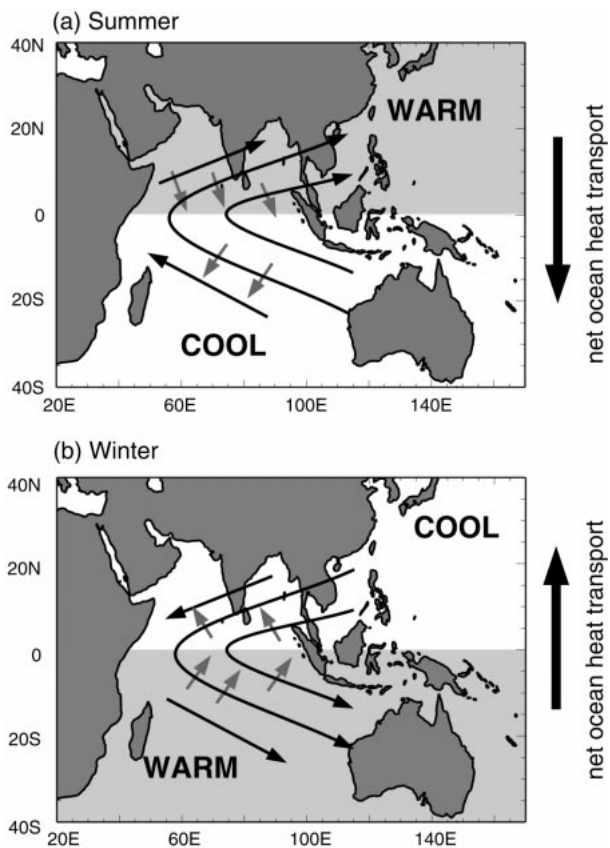
FIG. 13. A regulatory model of the annual cycle of the Indian Ocean monsoon system depicted for (a) summer (Jun–Sep) and (b) winter (Dec–Feb). Curved black arrows denote the wind forced by the large-scale differential heating denoted by "warm" and "cool." The small gray arrows are the Ekman transports forced by the winds. The large vertical black arrows to the right show the net ocean heat transport that reverses between boreal summer and winter. The net effect of the combined wind-forced ocean circulation is to transport heat to the winter hemisphere, thus modulating the SST differences between the hemispheres.

depicted as solid streamlines in Fig. 13a. The oceanic Ekman transport, associated with the monsoon winds are displayed as gray arrows with mass transports to the right of the wind direction in the Northern Hemisphere and to the left in the Southern Hemisphere. Because of the characteristics of the monsoon gyre (generally westward south of the equator and eastward to the north), the direction of the Ekman transport is to the south on both sides of the equator. As long as the Ekman flux is across a temperature gradient that is warm in the north and cool in the south in the boreal summer (see Figs. 7 and 8), there is a cross-equatorial heat transport to the Southern Hemisphere. In summary, excess heat accumulating in the upper ocean of the North Indian Ocean during the boreal spring and summer is advected southward. During the boreal winter (Fig. 13b) the reverse situation occurs. The monsoon gyre is counterclockwise and the meridional component of the atmospheric flow is to the south. Again, the Ekman transports on either

side of the equator are the same sign, collectively resulting in a northward oceanic heat transport across the equator.

A number of studies have shown that the magnitude of the Indian Ocean SST is a very important component of the monsoon system. Meehl (1987, 1997) relates the variability of the monsoon from one year to the next directly to the magnitude of the SST preceding the boreal summer. Meehl's observations have been corroborated by a number of studies (e.g., Hastenrath 1987; Harzallah and Sadourny 1997; Sadhuram 1997; and Clark et al. 2000), which have shown that Indian Ocean SST anomalies in the winter and spring correlate strongly with the strength of the following monsoon. The aforementioned studies refer principally to the interannual variability of the monsoon. Here we have examined primarily the annual cycle.

The importance of SST to the annual cycle of the monsoon is illustrated by the careful modeling experiments of Shukla and Fennessy (1994). In experiments that successively removed the annual cycle of the SST and the solar radiation, they were able to deduce the relative importance to the monsoon of the two primary external forcing fields of their model. In comparison with a control simulation, both experiments showed dramatic reductions in the monsoon rainfall over the Arabian Sea, India, the Bay of Bengal, and southeast Asia. The Shukla–Fennessy results show clearly that the annual cycle of SST in the northern Indian Ocean and land surface processes are both critical components of the monsoon system. Their results are particularly relevant to the problem of modeling of the coupled monsoon system. If a coupled ocean–atmosphere model is not capable of simulating the observed annual cycle of SST, it is unlikely whether the simulated monsoon circulation or the associated precipitation patterns would be accurate. In the preceding paragraphs, we have attempted to show how the annual cycle of SST in the Indian Ocean is determined in the context of the coupled ocean–atmosphere–land system.

6. Summary

We have used an ocean model of intermediate complexity to study the annual cycle of the Indian Ocean. Using the climatological mean COADS dataset to force the model, it is found that large positive surface heat flux into the northern Indian Ocean during the boreal spring and early summer is balanced by both increases in heat storage of the upper ocean as well as net southward transports of heat across the equator. During the winter, the SST in the North Indian Ocean is modulated by oceanic heat transports from the Southern Hemisphere. In the Indian Ocean during the spring and early summer, warm SSTs are not accompanied by convection as they are in the Pacific. Cross-equatorial heat transport has been shown to be the primary process for both the
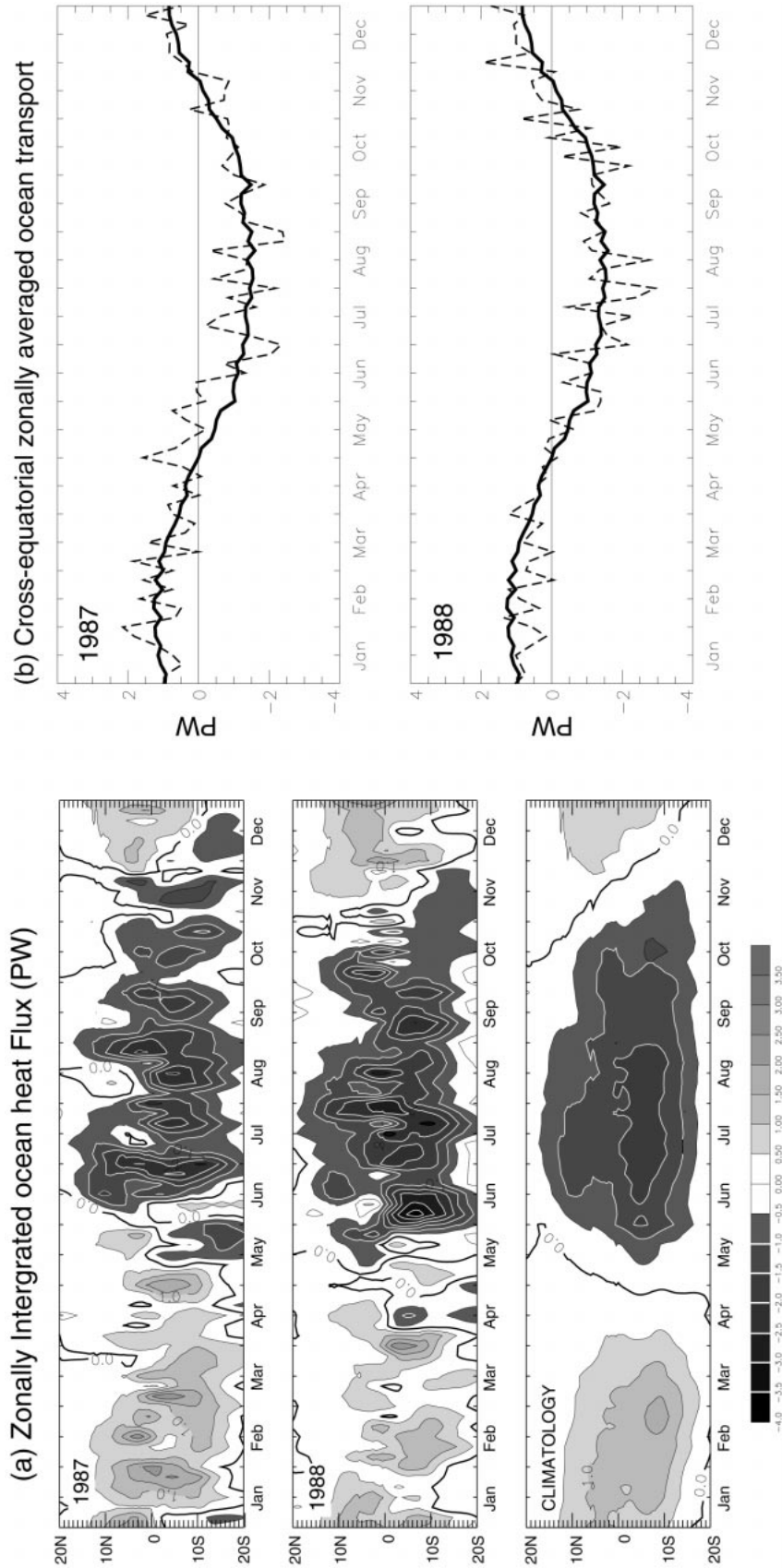
FIG. 14. Time–latitude sections of total meridional ocean heat transport for (a) 1987, 1988, and the long-term climatology; and (b) the average 5°N–5°S ocean heat transport plotted for 1987 and 1988 vs climatology. The model was forced by 5-day average NCEP surface winds (Kalnay et al. 1996).
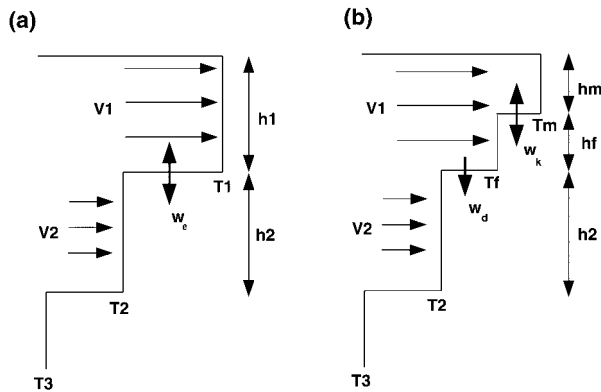
(a) **(b)**

Fig. 15. Schematic of model layers as in McCreary et al. (1993). (a) The mixed layer spreads throughout the upper layer of thickness h_1 and temperature T_1. (b) The upper layer consists of a mixed layer of thickness h_m and temperature T_m overlying a fossil layer of thickness h_f and temperature T_f, with mean temperature being T_1. Here T_2 is the lower-layer temperature, and T_3 is the temperature of the deep, inert ocean.

modulation of the heat balance and the regulation of the SST in the northern part of the basin.

In comparing the dynamics and thermodynamics of the northern Indian Ocean to the western Pacific Ocean warm pool, one can consider oceanic heat transport to be part of a suite of processes that modulate warm pool SST. If the system is so configured that thermodynamical processes are sufficiently rapid then the system will adjust toward equilibrium thermodynamically in the manner of the thermostat hypothesis (Ramanathan and Collins 1991). If these processes are too slow, then other processes such as atmospheric transports of heat may occur. If thermodynamical processes (cloud feedbacks) or atmospheric processes (enhanced evaporation) are not of sufficient strength to regulate SST due to local constraints (such as the externally forced subsidence over the North Indian Ocean), the upper ocean can only relax through oceanic transport processes. The western Pacific Ocean and the northern Indian Ocean offer two different examples of a system relaxing toward equilibrium.

During the course of this study, much has been made of the difference between the north Indian and tropical western Pacific Oceans. Specifically, the comparison has been made between the warm pools of the two ocean basins rather than the entire tropical extent of the basins that would include the South Indian and the East Pacific Ocean. The reason for the choosing the warm pools rather than the entire tropical basins was to match the same region of the Pacific as other studies (e.g., Ramanathan and Collins 1991). The North Indian Ocean region was chosen because of the importance of its SST to the overall annual cycle of the monsoon (Meehl 1987, 1997). Furthermore, neither the North Indian Ocean nor the western Pacific warm pools were considered in isolation. The North Indian Ocean was considered in concert with the South Indian Ocean through connections of basin-scale wind forcing that determines the heat

transport. Similarly, the tropical western and eastern Pacific Ocean was assumed to be connected through the large-scale Walker circulation.

With respect to the comparison of Pacific and Indian Ocean warm pools, a number of points can be made.

1) Very large transequatorial transports of heat are necessary to balance the heat budget of the north Indian Ocean on a seasonal basis. These transports are of the same order as the net surface heating of the northern basin and vary between ±1.5 PW between winter and summer, respectively. Without these imports and exports of heat, the annual cycle of SST over the entire Indian Ocean basin would be much larger.
2) The annual average heat transport across the equator in the Indian Ocean is about an order of magnitude smaller than the extremes of the annual cycle and matches the net accumulation of heat in the North Indian Ocean (Fig. 12b).
3) It is probable that in the Pacific Ocean warm pool that oceanic heat advection cannot be neglected on seasonal to interannual timescales (Sun and Liu 1996; Clement et al. 1996). However, assuming that balances are achieved by lateral transports of heat by the ocean out of the tropical western Pacific warm pool (defined by the areal extent of the 28°C isotherm) on an annual basis, they would be about 10% of the peak across the equator in the Indian Ocean. This calculation is based on a net surface flux of 15 W m^{-2} into the tropical western Pacific warm pool (Godfrey et al. 1998) and no change in heat storage over the year. Clement et al. (1996), however, state that oceanic advection of heat is most important in the eastern Pacific Ocean, and that the western Pacific Ocean SST is determined by a one-dimensional balance of surface flux and storage.
4) Assuming that the excess heat flux in the western Pacific Ocean is transported out of the warm pool each year, the net annual transport out of the northern Indian Ocean and the tropical warm pool are roughly equal. But the surface heat flux into the tropical western Pacific is essentially constant throughout the year with a relatively small annual cycle. Over the northern Indian Ocean the integrated surface flux varies between −0.5 and +0.75 PW (Fig. 5a) and the large cross-equatorial oceanic heat transports are essential to keeping the upper ocean heat balance within bounds. Furthermore, Lukas (1988) argues that the excess heat flux into the tropical western Pacific Ocean is not exported annually but accumulated. Lukas (1988) speculates that this accumulation leads to interannual oscillations.

The last point requires further discussion. If only the annual net heat flux into the Indian Ocean and the tropical western Pacific Ocean are considered, the two warm pools appear very similar. However, considering only the annual average of the Indian Ocean would preclude consideration of the very large annual cycle of the In-

dian Ocean heat balance that is a critical element in the evolution of the Asian monsoon system. Ignoring the annual cycle in the North Indian Ocean would be similar to considering the mean annual monsoon circulation in the atmosphere. Tomczak and Godfrey (1994) show the Sverdrup transports driven by a mean annual wind field. In the annual mean, the North Indian Ocean is a region with weak cross-equatorial heat transport. From this annual averaged perspective, the North Indian Ocean is indistinguishable from the tropical western Pacific. In the latter region, where there is a very small annual cycle of wind and surface heating (Table 1), the ocean is forced by the annual averaged wind and heating is representative of the seasonal character. However, this is clearly not the case in the Indian Ocean.

Despite the compensation of the extremes of the annual cycle in the Indian Ocean, there is also large interannual variability resulting from long-term changes in surface forcing (Fig. 12). It was also noted that the system seemed to equilibrate within relatively narrow bounds even if the surface forcing varied substantially from year to year. This equilibration can perhaps be explained in terms of the coupled ocean–atmosphere–land model of the Indian Ocean monsoon system described in section 5.

Whether or not the coupled ocean–atmosphere regulatory system, described in Fig. 13 and section 5, can help explain the interannual variability of the monsoon system, such as the biennial oscillation described by Meehl (1987, 1997), is currently under investigation. In particular we are interested in the manner in which the monsoon system responds to variations in the large-scale forcing. Such variations may occur from the influence of the phase of ENSO (e.g., Shukla and Paolina 1983), more or less persistent winter snowfall over Eurasia (e.g., Yasunari et al. 1991; Vernekar et al. 1995), SST anomalies, stochastic processes in the southern Indian Ocean (Rodwell 1997), or perhaps through chaotic processes (Palmer 1994). For example, it is interesting to speculate on what would occur if the large-scale monsoon pressure gradient were reduced (or strengthened) by one of the processes described above, in the context of the simple regulatory monsoon model.

Ocean variability on timescales less than seasonal have not been addressed in this paper. However, considerable intraseasonal variability has been noted in the Indian Ocean together with large-scale changes in SST (Fasullo and Webster 1999). As the intraseasonal variations occur with accelerations and decelerations of the monsoon gyre (Webster et al. 1998), a wind-driven signal in the ocean can be expected. Figures 14a–c show cross-equatorial heat transports plotted as a function of latitude and time for the long-term climatology and for the specific years 1987 and 1988, respectively. The model was forced by 5-day mean winds from the NCEP–NCAR reanalysis dataset. Superimposed on the annual cycle are large oscillations on timescales ranging for 20 days or so to the timescales of the active and break periods of the monsoon. For example, during the summer, when the mean oceanic heat transport is in excess of −1 PW, variations on the 20–50-day timescale occur with peaks and valleys ranging between −4 and +0.5 PW, respectively. Extrema of the cross-equatorial transports coincide with the active and break phases of the South Asian monsoon listed in Webster et al. (1998), but there are oscillations that also occur on timescales that are about half of this period. Whether or not these are forced modes, instability modes [such as those described by Kindle and Thompson (1989) for the western Indian Ocean], or combinations of both remains to be seen. The intraseasonal variability of the coupled ocean–atmosphere system will be considered in greater detail in a separate paper. The model we intend to use for this future work will be the 4½ level model of Han et al. (1999). The high-frequency variability and climatology of the Han et al. (1999) model are quite similar to those of the model used in this study, but the added vertical resolution will allow an easier definition of the relative roles of eddies and meridional overturnings in accomplishing oceanic heat transports.

A final question refers to the vastly different radiative forcing between the North Indian Ocean and the tropical western Pacific. Why is there an absence of clouds in the North Indian Ocean during spring even though the SST is very high? The answer is probably related to the geography of the region. The North Indian Ocean is surrounded on its northern and western side by very arid regions. During the boreal spring these regions are radiative sinks to space (high values of OLR in Fig. 1b). In order to counterbalance the loss of heat to space, strong subsidence is necessary (Stephens and Webster 1981). In turn, the subsidence inhibits convection over the northwestern Indian Ocean. In contrast, the western Pacific Ocean does not possess large continental regions and the atmosphere structure is dominated by the warm SSTs, the release of latent heat, and the minimization of longwave radiation loss by the depth of deep convection (low values of OLR in Fig. 1b).

The ability to observe accurately the heat balance of the Indian Ocean over a complete annual cycle, as well as variability on longer timescales, would be of great benefit to increasing predictive skills within the Indian Ocean monsoon region. Initial process studies have been undertaken in the eastern Indian Ocean by Hacker et al. (1998) and in the recently completed JASMINE.[5] The main purpose of JASMINE is to understand the variation of ocean–atmosphere interaction during the active and break periods of the monsoon. The documentation of the surface energy balance over a wide range of conditions was an important achievement.

---

[5] Details of JASMINE together with initial results from the field phase can be found online at http://paos.colorado.edu/~jasmine.

APPENDIX

Model Description

To investigate the response of the Indian Ocean to the surface forcing, we use the McCreary et al. (1993) ocean model that has been shown to simulate successfully many of the circulation features of the upper Indian Ocean. The McCreary et al. model resolves many details of the Indian Ocean annual cycle, as well as replicating the seasonally reversing meridional circulation cell that dominates the heat transport in this region. Since the annual cycle and basic features of the Indian Ocean are well reproduced by a relatively simple 2½ layer model, we choose this intermediate model over more complex multilayer or ocean GCM models so as to simulate the seasonal variability in the upper ocean in a manner that is less dynamically complex, but yet reveals fluctuations in the heat balance on seasonal timescales.

The basic structure of the model is shown in Fig. 15, with the two possible vertical structures displayed. Basic descriptions of the model found here are taken from McCreary et al. (1993). In one possible scenario, the surface layer is a single layer with thickness h_1, velocity v_1, and temperature T_1. During periods of detrainment, when the mixed layer retreats due to low winds or surface heating, the upper layer can split into a mixed layer, with thickness h_m and temperature T_m, and a nonturbulent "fossil layer" of thickness h_f and temperature T_f. In the case of the split, the velocity field v_1, however, is still assumed to be slablike, so that the shear between the mixed and fossil layers is always neglected. The lower layer has thickness h_2, velocity v_2, and temperature T_2, and is in the depth range of the thermocline. The temperature of the deep inert ocean is T_3, which is set to a constant of 4°C.

The mixed layer entrains ($w_k > 0$) or detrains ($w_k < 0$) water according to the Kraus–Turner method (Kraus and Turner 1967), where mixing is maintained by surface turbulence caused by wind mixing and surface cooling. The fossil layer is isolated from the surface turbulence, but can be engulfed into the mixed layer (Fig. 15a) either during periods of strong entrainment by w_k or in upwelling regions where h_1 shallows significantly. Because there is considerable entrainment into the upper layer, there must also be detrainment ($w_d < 0$) through the base of the upper layer for mass continuity. This process simulates the subduction of surface layer water into the thermocline.

In all the model runs, the thermal forcing is defined by (5) where the turbulent fluxes are computed using standard bulk formulas from the fields of air temperature T_a, specific humidity q_a, and scalar wind v_a provided by the atmospheric forcing, with model surface temperature T_m used for the temperature of the ocean layer in contact with the atmosphere. Wind stress is applied to the upper model layer, and is calculated from the wind fields using a standard bulk formula.

The model domain extends from 29°S to 25°N, and from 35° to 115°E, and uses realistic lateral geographic boundaries representing the African, Asian, and Indonesian coasts. The western, northern, and eastern boundaries are considered closed, so that no throughflow exists from the eastern boundary. The southern boundary (29°S) of the model is an open boundary, where zero-gradient, open boundary conditions are applied, and where fluid can pass across the southern model limits. For a discussion of the southern boundary details and their affect on the model heat budget, see McCreary et al. (1993).

Solutions to the model are found numerically on a rectangular grid with a grid spacing of $x = y = 55$ km. Equations are integrated forward in time with a time step of 1 h. The model is spun up from a state of rest beginning on 15 April, which climatologically is a weak wind period in the northern Indian Ocean. To inhibit the excitation of inertial oscillations, the wind stress driving the model is ramped up from zero to the observed level over a 5-day period. The model is spun up from a state of rest for a period of 9 yr, by which time it reached a stable annual cycle. All model output is taken from year 10 of integration.

REFERENCES

Arkin, P., and B. Meisner, 1987: The relationship between large-scale convective rainfall and cloud cover over the western hemisphere during 1982–1984. *Mon. Wea. Rev.,* **115,** 51–74.

Bishop, J. K. B., and W. B. Rossow, 1991: Spatial and temporal variability of global surface solar irradiance. *J. Geophys. Res.,* **96,** 16 839–16 858.

Boning, C. W., and F. O. Bryan, 1996: Large-scale transport processes in the high-resolution circulation models. *The Warm Water Sphere of the North Atlantic Ocean,* W. Kraus, Ed., Gebruder Borntrager, 91–127.

CEPEX, 1993: Central Equatorial Pacific Experiment, experiment design. Tech. Report, Scripps Institution of Oceanography, 54 pp. [Available from Center for Clouds, Chemistry and Climate, Scripps Institution of Oceanography, UCSD, 9500 Gilman Dr. #0221, La Jolla, CA 92093.]

Clark, C. O., J. E. Cole, and P. J. Webster, 2000: Indian Ocean SST and Indian summer rainfall: Predictive relationships and their decadal variability. *J. Climate,* **13,** 2503–2519.

Clement, A., R. Seager, M. A. Cane, and S. E. Zebiak, 1996: An ocean dynamical thermostat. *J. Climate,* **9,** 2190–2196.

Fasullo, J. T., and P. J. Webster, 1999: Warm pool SST variability in relation to the surface energy balance. *J. Climate,* **12,** 1292–1305.

——, and ——, 2000: Atmospheric and surface variations during

westerly wind bursts in the tropical western Pacific. *Quart. J. Roy. Meteor. Soc.,* **126,** 899–924.

Fu, R., A. D. del Genio, W. B. Rossow, and W. T. Liu, 1992: Cirrus-cloud thermostat for tropical sea surface temperatures tested using satellite data. *Nature,* **358,** 394–397.

Garternicht, U., and F. Schott, 1997: Heat fluxes of the Indian Ocean from a global eddy-resolving model. *J. Geophys. Res.,* **102,** 21 147–21 159.

Gill, A., 1982: *Atmosphere–Ocean Dynamics.* International Geophysics Series, Vol. 30, Academic Press, 662 pp.

Godfrey, J. S., 1996: The effect of the Indonesian throughflow on ocean circulation and heat exchange in the atmosphere: A review. *J. Geophys. Res.,* **101,** 12 217–12 237.

——, R. A. Houze Jr., R. H. Johnson, R. Lukas, J. L. Redelsperger, A. Suomi, and R. Weller, 1998: Coupled Ocean–Atmosphere Response Experiment (COARE): An interim report. *J. Geophys. Res.,* **103,** 14 395–14 450.

Hacker, P., E. Firing, J. Hummon, A. Gordon, and J. C. Kindle, 1998: Bay of Bengal currents during the northeast monsoon. *Geophys. Res. Lett.,* **25,** 2769–2772.

Hall, M. M., and H. L. Bryden, 1982: Direct estimates and mechanisms of ocean heat transport. *Deep-Sea Res.,* **29,** 339–359.

Han, W., J. P. McCreary, D. L. T. Anderson, and A. J. Mariano, 1999: Dynamics of the eastern surface jets in the equatorial Indian Ocean. *J. Phys. Oceanogr.,* **29,** 2191–2209.

Hartmann, D. L., and M. L. Michelsen, 1993: Large-scale effects on the regulation of tropical sea surface temperatures. *J. Climate,* **6,** 2049–2062.

Harzallah, R., and R. Sadourny, 1997: Observed lead–lag relationships between Indian summer monsoon and some meteorological variables. *Climate Dyn.,* **13,** 635–648.

Hastenrath, S., 1987: On the prediction of India summer rainfall anomalies. *J. Climate Appl. Meteor.,* **26,** 847–857.

——, and P. J. Lamb, 1979a: *Surface Climate and Atmospheric Circulation.* Vol. 1, *Climatic Atlas of the Indian Ocean,* University of Wisconsin Press, 116 pp.

——, and ——, 1979b: *Oceanic Heat Budget.* Vol. 2, *Climatic Atlas of the Indian Ocean,* University of Wisconsin Press, 110 pp.

——, and L. Greischar, 1989: *Upper Ocean Structure.* Vol. 3, *Climatic Atlas of the Indian Ocean,* University of Wisconsin Press, 273 pp.

——, and ——, 1993: The monsoonal heat budget of the hydrosphere–atmosphere system in the Indian Ocean sector. *J. Geophys. Res.,* **98,** 6869–6881.

Hirst, A. C., and J. S. Godfrey, 1993: The role of Indonesian throughflow in a global ocean GCM. *J. Phys. Oceanogr.,* **23,** 1057–1086.

Kalnay, E., and Coauthors, 1996: The NCEP/NCAR 40-Year Reanalysis Project. *Bull. Amer. Meteor. Soc.,* **77,** 437–471.

Kantha, L. H., and C. A. Clayson, 1994: An improved mixed layer model for geophysical applications. *J. Geophys. Res.,* **99,** 25 235–25 266.

Kindle, J. C., and J. D. Thompson, 1989: The 26- and 50-day oscillations in the western Indian Ocean: Model results. *J. Geophys. Res.,* **94,** 4721–4736.

Knox, R. A., 1986: The Indian Ocean: Interaction with the monsoon. *Monsoons,* J. S. Fein and P. L. Stephens, Eds., Wiley-Interscience, 365–398.

Kraus, E. B., and J. S. Turner, 1967: A one-dimensional model of the seasonal thermocline II: The general theory and its consequences. *Tellus,* **19,** 98–106.

Lau, K.-M., and C.-H. Sui, 1997: Mechanisms of short-term sea surface temperature regulation: Observations during TOGA COARE. *J. Climate,* **10,** 465–472.

Lee, T., and J. Marotzke, 1997: Inferring meridional mass and heat transports of the Indian Ocean by fitting a general circulation model to climatological data. *J. Geophys. Res.,* **102,** 10 585–10 602.

Levitus, S., 1982: *Climatological Atlas of the World Ocean.* NOAA Prof. Paper 13, 163 pp. and 17 microfiche.

——, 1987: Meridional Ekman heat fluxes for the world ocean and individual ocean basins. *J. Phys. Oceanogr.,* **17,** 1484–1492.

Lukas, R., 1988: On the role of western Pacific air–sea interaction in the El Niño/Southern Oscillation phenomenon. *Proc. U.S. TOGA Western Pacific Air–Sea Interaction Workshop,* Honolulu, HI, University Corporation for Atmospheric Research, 43–69. [UCAR Tech. Rep. US-TOGA-8.]

McCreary, J. P., Jr., P. K. Kundu, and R. L. Molinari, 1993: A numerical investigation of dynamics, thermodynamics and mixed-layer processes in the Indian Ocean. *Progress in Oceanography,* Vol. 31, Pergamon, 181–244.

Meehl, G. A., 1987: The annual cycle and interannual variability in the tropical Pacific and Indian Ocean regions. *Mon. Wea. Rev.,* **115,** 27–50.

——, 1997: The south Asian monsoon and the tropospheric biennial oscillation. *J. Climate,* **10,** 1921–1943.

National Research Council, 1994: *GOALS (Global Ocean–Atmosphere–Land System) for Predicting Seasonal-to-Interannual Climate.* National Academy Press, 103 pp.

Oberhuber, J. M., 1988: An atlas based on the COADS data set: The budgets of heat, buoyancy and turbulent kinetic energy at the surface of the global ocean. Max-Planck-Institut für Meteorologie Tech. Rep. 15, 20 pp. [Available from Max-Planck-Institut für Meteorologie, Bundesstrasse 55, 20146 Hamburg, Germany.]

Palmer, T. N., 1994: Chaos and the predictability in forecasting the monsoons. *Proc. Indian Nat. Sci. Acad., Part A,* **60,** 57–66.

——, and D. A. Mansfield, 1984: Response of two atmospheric general circulation models to sea-surface temperature anomalies in the tropical east and west Pacific. *Nature,* **310,** 483–485.

Ramanathan, V., and W. Collins, 1991: Thermodynamic regulation of ocean warming by cirrus clouds deduced from observations of the 1987 El Niño. *Nature,* **351,** 27–32.

Rayner, N. A., E. B. Horton, D. E. Parker, C. K. Folland, and R. B. Hackett, 1996: Version 2.2 of the global sea-ice and sea surface temperature data set, 1903–1994. Tech. Rep. CRTN 74, Hadley Centre for Climate Prediction and Research, The Met. Office, 14 pp. [Available from Hadley Centre for Climate Prediction and Research, The Met. Office, London Road, Bracknell, Berkshire RG12 2SY, United Kingdom.]

Rodwell, M. J., 1997: Breaks in the Asian monsoon: The influence of Southern Hemisphere weather systems. *J. Atmos. Sci.,* **54,** 2597–2611.

Sadhuram, Y., 1997: Predicting monsoon rainfall and pressure indices from sea surface temperature. *Curr. Sci.,* **72,** 166–168.

Shukla, J., and D. A. Paolina, 1983: The southern oscillation and long-range forecasting of the summer monsoon rainfall over India. *Mon. Wea. Rev.,* **111,** 1830–1837.

——, and M. J. Fennessy, 1994: Simulation and predictability of monsoons. Proceedings of the International Conference on Monsoon Variability and Prediction, Tech. Rep. WCRP-84, World Climate Research Programme, Geneva, Switzerland, 567–575.

Stephens, G. L., and P. J. Webster, 1981: Clouds and climate: Sensitivity to simple systems. *J. Atmos. Sci.,* **38,** 235–247.

——, and T. Slingo, 1992: An air-conditioned greenhouse. *Nature,* **358,** 369–370.

Sun, D.-Z., and Z.-Y. Liu, 1996: Dynamic ocean–atmosphere coupling: A thermostat for the Tropics. *Science,* **272,** 1148–1150.

TOGA COARE International Project Office, 1994: Summary report of the TOGA COARE International Data Workshop. Toulouse, France. [Available online at www.ncdc.noaa.gov/coare/meetings/wkshp_rpt/report.html.]

Tomczak, M., and J. S. Godfrey, 1994: *Regional Oceanography: An Introduction.* Pergamon, 422 pp.

Torrence, C., and P. J. Webster, 1999: Interdecadal changes in the ENSO–monsoon system. *J. Climate,* **12,** 2679–2690.

Vernekar, A. D., J. Zhou, and J. Shukla, 1995: The effect of Eurasian snow cover on the Indian monsoon. *J. Climate,* **8,** 248–266.

Wacongne, S., and R. C. Pacanowski, 1996: Seasonal heat transport in the tropical Indian Ocean. *J. Phys. Oceanogr.,* **26,** 2666–2699.

Wallace, J. M., 1992: Effect of deep convection on the regulation of tropical sea surface temperature. *Nature,* **357,** 230–231.

WCRP, 1985: Scientific plan for the Tropical Ocean Global Atmosphere Programme. WCRP Publication 3, World Meteorological Organization, Geneva, Switzerland, 146 pp.

Webster, P. J., 1987: The elementary monsoon. *Monsoons,* J. S. Fein and P. L. Stephens, Eds., Wiley-Interscience, 3–32.

——, 1994: The role of hydrological processes in ocean–atmosphere interactions. *Rev. Geophys.,* **32,** 427–476.

——, and R. Lukas, 1992: TOGA COARE: The Coupled Ocean–Atmosphere Response Experiment. *Bull. Amer. Meteor. Soc.,* **73,** 1377–1416.

——, and S. Yang, 1992: Monsoon and ENSO: Selectively interactive systems. *Quart. J. Roy. Meteor. Soc.,* **118,** 877–926.

——, J. A. Curry, and C. A. Clayson, 1996: Clouds, radiation, and the diurnal variation of sea surface temperature in the tropical western pacific. *J. Climate,* **9,** 1712–1730.

——, T. Palmer, M. Yanai, V. Magana, J. Shukla, R. A. Tomas, M. Yanai, and A. Yasunari, 1998: Monsoons: Processes, predictability and the prospects for prediction. *J. Geophys. Res.,* **103** (C7), 14 451–14 510.

——, A. Moore, J. Loschnigg, and M. Leban, 1999: Evidence of coupled ocean–atmosphere interactions in the Indian Ocean. *Nature,* **401,** 356–360.

Yasunari, T., A. Kitoh, and T. Tokioka, 1991: Local and remote responses to excessive snow mass over Eurasia appearing in the northern spring and summer climate: A study with the MRI-GCM. *J. Meteor. Soc. Japan,* **69,** 473–487.